Pergamon

Cement and Concrete Research 30 (2000) 411–418

CEMENT AND CONCRETE RESEARCH

Chemical changes in concrete due to the ingress of aggressive species

P.W. Brown[a,*], April Doerr[b]

[a]Department of Materials Science and Engineering, Penn State University, University Park, PA 16802, USA
[b]R.J. Lee Group, Monroeville, PA 15146, USA

Received 1 July 1999; accepted 17 December 1999

Abstract

Chemical changes in field concretes due to the ingress of sodium, magnesium, sulfate, chloride, and carbonate are analyzed. Each of these species participated in the deterioration of these concretes. Magnesium compounds formed were brucite and magnesium silicate hydrates. Sulfate form gypsum, ettringite, and thaumasite. Chloride intrusion permitted the formation of Friedel's salt. Finally, sodium carbonate was formed. The mechanisms by which these compounds were formed are discussed. © 2000 Elsevier Science Inc. All rights reserved.

Keywords: Ettringite formation; Sulfate attack; Friedel's salt formation; Magnesium silicate formation; Sodium carbonate formation

1. Introduction

In the late 1980s, concrete foundations in homes in southern California were observed to be undergoing sulfate attack. Sulfate attack of concrete foundations of homes in this region was documented, and a variety of compounds not typically observed in concrete were detected [1,2]. In particular, the nature of attack in homes in the cities of La Palma, Lakewood, and Cypress, CA was documented. Among the compounds identified in concretes from these homes are: Na_2SO_4 (thenardite), $Na_2SO_4{\cdot}10H_2O$ (mirabilite), $Na_3H(CO_3)_2{\cdot}2H_2O$ (trona), $Na_2CO_3{\cdot}H_2O$ (thermonatrite), and $NaHCO_3$ (nahcolite). Also identified were $CaSO_4{\cdot}2H_2O$, $CaCO_3$, $CaSiO_3{\cdot}CaCO_3{\cdot}CaSO_4{\cdot}15H_2O$ (thaumasite) and $8.5CaSiO_3{\cdot}9.5CaCO_3{\cdot}CaSO_4{\cdot}15H_2O$ (bircunite), $Na_3(NO_3)(SO_4){\cdot}H_2O$, $NaNO_3$, and NaCl.

As pointed out by Haynes et al. [3], sodium sulfates can result in a damage to the concrete due to cyclic formation of the anhydrous and hydrated forms of these salts. For exposure conditions, which do not involve direct contact with the soil or the accumulation of water due to run-off, the formation of these forms of efflorescence is indicative of the movement of sodium and sulfate through the concrete pore structure. Under such circumstances, the formation of sodium sulfate on a concrete surface is an indication of sulfate attack occurring in the interior of that concrete; the distributions of sulfate-containing phases have been discussed in detail elsewhere [4].

The formation of a sodium carbonate may also be indicative of sulfate attack as illustrated by the following reactions [Eqs. (1,2)]:

$$Na_2SO_{4aq} + Ca(OH)_2(s) \Rightarrow 2NaOH_{aq} + CaSO_4 \cdot 2H_2O(s) \quad (1)$$

$$NaOH_{aq} + HCO_{3aq} \Rightarrow Na_{(2-x)}H_xCO_3 \cdot (nH_2O) \quad \text{where } x = 0,\ 0.5,\ \text{or } 1. \quad (2)$$

The gypsum formed according to Eq. (1) is available to react with aluminate-containing phases to form ettringite.

More recently, the occurrence of sulfate attack in homes constructed within the last 10 years has been documented. The homes from which concretes were obtained for the present study were built on soils which were an ancient seabed. As a consequence, the soil in contact with these concretes contains significant quantities of the soluble salts NaCl, Na_2SO_4, and $MgSO_4$.

The concretes examined were obtained from homes in a development in Southern California were built on a hillside facing the Pacific Ocean. Prior to construction, the standard practice of cutting and filling to produce the grading required for roads, driveways, footings, and garage slabs was carried out. The homes themselves were built into the hillsides and their foundations are comprised of retaining walls, foundation piers, and stem walls. Although Type V

* Corresponding author. Tel.: +1-814-865-5352; fax: +1-814-863-7040.
E-mail address: etx@psu.edu (P.W. Brown).

PII: S0008-8846(99)00266-5

concrete was used, the average water-to-cement ratio was determined to be in the range of 0.65–0.70 [5]. The elevated water-to-cement ratio used permitted the ingress of aggressive species and efflorescence was routinely observed on the evaporative surfaces of concrete members. The objective of this paper is to describe the observations which were made regarding the nature of the compounds formed in the context of their distributions in these concretes. In particular, the mechanisms leading to the distributions of thaumasite, sodium carbonate(s), Friedel's salt, magnesium silicates, and $Mg(OH)_2$ observed in the concretes are discussed.

2. Experimental

One sample of concrete analyzed in this study was obtained from a reinforced foundation pier approximately 18 in. in diameter. A 4-in. diameter core about 11 in. in length was drilled approximately horizontally in the pier at a location about 6 in. above the soil line. A second sample of concrete was cored from a 6-in. thick stem wall foundation of another home. A 4-in. core of this concrete was also obtained from above the soil line.

The cores were slabbed using a diamond wheel saw. For the pier, three segments, each approximately 1-cm thick, were taken along the length of the core. Each segment was about 50 mm in length. One segment extended from the surface to a depth of about 50 mm, the second was taken from about 13 cm below the surface and the final segment was taken from about 25 cm below the surface. Two slabs were cut from the stem wall core. Each was approximately 50 mm in length and extended from the outside and inside surfaces. These slabs were dried and vacuum impregnated with epoxy using a method described by Jakobsen et al. [6]. Thin sections were then prepared in the usual manner [7] from these slabs by diamond wheel sawing and polishing. After carbon coating, the distributions of Mg, Cl and S in these thin sections were established by microprobe. Profiles across each thin section from the outside of the core to the inside were established by measuring the k ratios for each of these

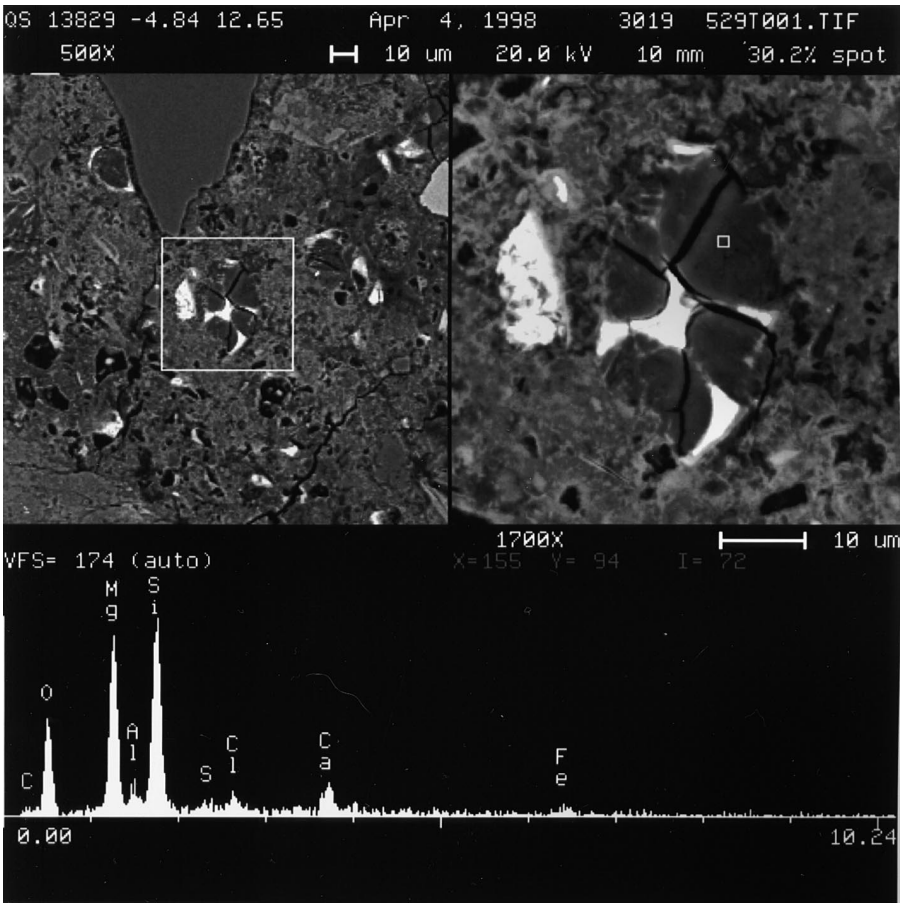

Fig. 1. A microstructure illustrating elevated paste porosity in the concrete. The central feature shows magnesium silicate pseudomorphs of former belite grains. The EDS spectrum of this former belite grain shows it has completely decalcified and converted to a magnesium silicate.

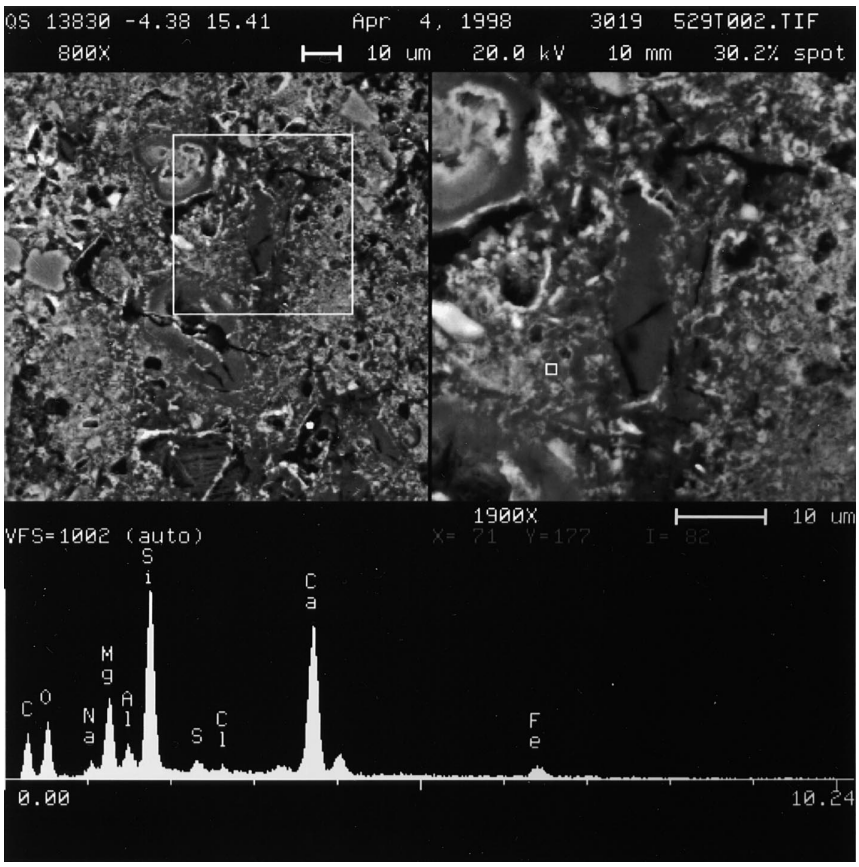
QS 13830 -4.38 15.41 Apr 4, 1998 3019 529T002.TIF
800X 10 um 20.0 kV 10 mm 30.2% spot
1900X 10 um
VFS=1002 (auto) X= 71 Y=177 I= 82
C
O
Na
Mg
Al
Si
S
Cl
Ca
Fe
0.00
10.24

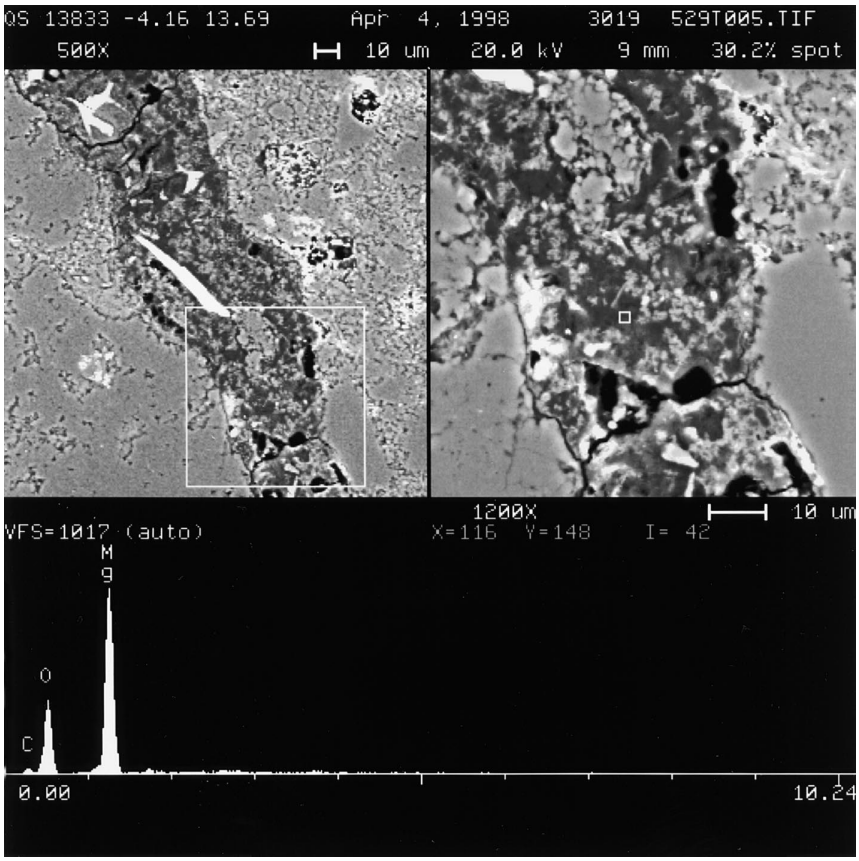
QS 13833 -4.16 13.69 Apr 4, 1998 3019 529T005.TIF
500X 10 um 20.0 kV 9 mm 30.2% spot
1200X 10 um
VFS=1017 (auto) X=116 Y=148 I= 42
C
O
Mg
0.00
10.24

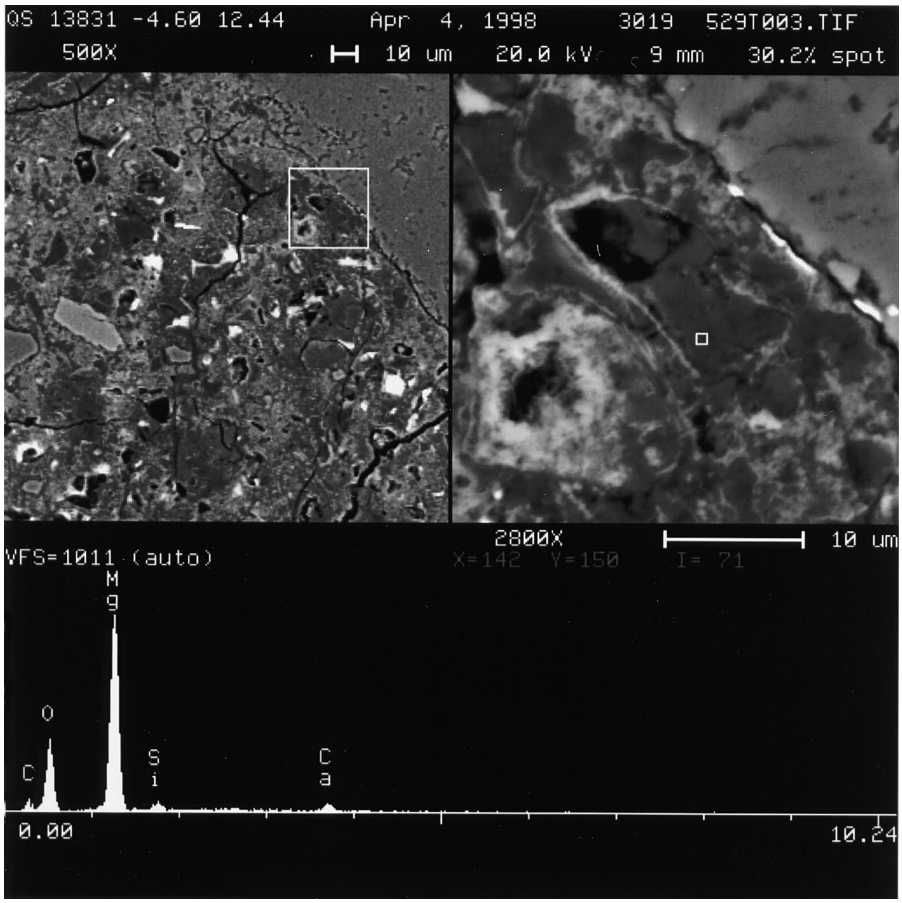

Fig. 2. (a) Mg enrichment of the paste; (b) $Mg(OH)_2$ pseudomorphs of $Ca(OH)_2$ in the paste; (c) $Mg(OH)_2$ replacing $Ca(OH)_2$ at the paste–aggregate interface.

elements in fields approximately 70–90 μm in size. Averages of five fields, each at about the same depths formed in the core surface were used to estimate the relative abundances across each thin section. Measurements were made at approximately every 4 mm across each thin section.

The distributions of Mg, Cl, and S established by the microprobe profiles were correlated with microstructural observations and with energy dispersive spectra of the microstructural features observed.

3. Results and discussion

Fig. 1 shows a typical microstructure illustrating the elevated paste porosity in the concrete from the foundation pier. Consistent with elevated porosity, the near-surface region of the pier is heavily carbonated. In addition, the CSH and the former cement grains have decalcified. Also associated with the elevated porosity is a profusion of Mg throughout the concrete. Microprobe analysis showed high Mg counts throughout the thin sections. Its effect is readily observed in Fig. 1. The EDS spectrum of this former belite grain shows both the absence of calcium and the accumulation of magnesium. Thus, this calcium silicate has converted to a magnesium silicate. The formation of magnesium silicate in Type V cement mortar exposed to magnesium sulfate has been reported by Gollup and Taylor [8]. Magnesium silicate formation in concrete exposed to seawater was reported by Cole [9] and by Roy et al. [10]. However, the formation of Mg-rich phases is normally associated with the near surface regions of concrete exposed to Mg-containing solutions, such as seawater. The formation of Mg silicates in this field concrete specimen required Mg to be transported a significant distance through the pore structure.

Typical of the interaction of Mg with concrete is the following base exchange reaction:

$$Mg^{2+} + Ca(OH)_2(s) \Rightarrow Mg(OH)_2(s) + Ca^{2+} \quad (3)$$

and the near-surface precipitation of $Mg(OH)_2$ is frequently observed [11,12]. Fig. 2a and the related EDS spectrum show a region of paste where there is significant Mg enrichment. Fig. 2b and the related spectrum show

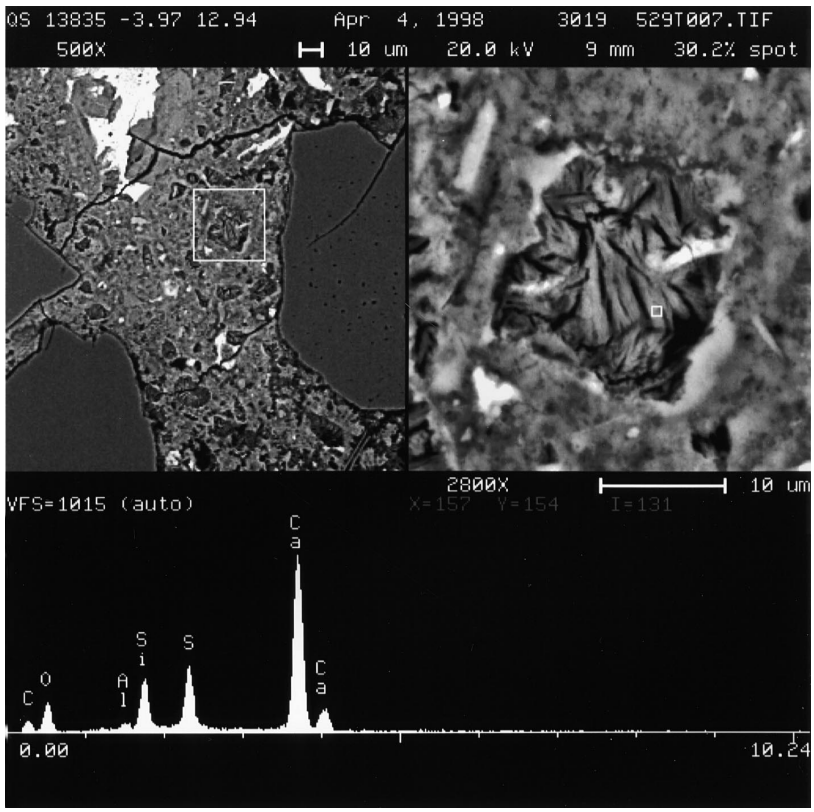

Fig. 3. The morphology typical of thaumasite and the EDS spectrum confirming thaumasite.

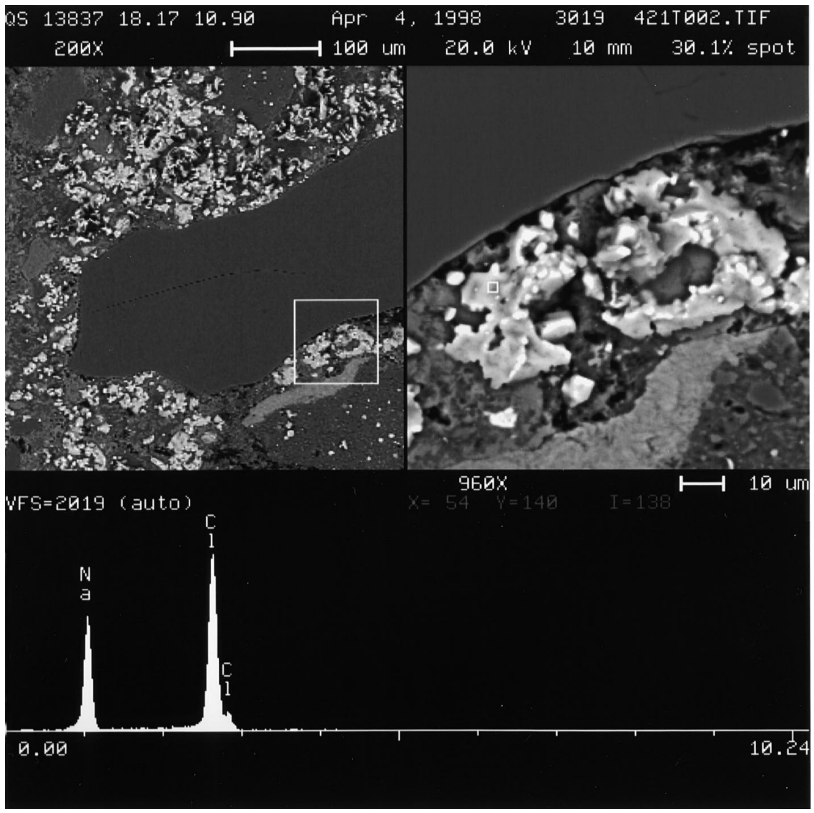

Fig. 4. The crystallization of NaCl within the paste and at the paste–aggregate interface.

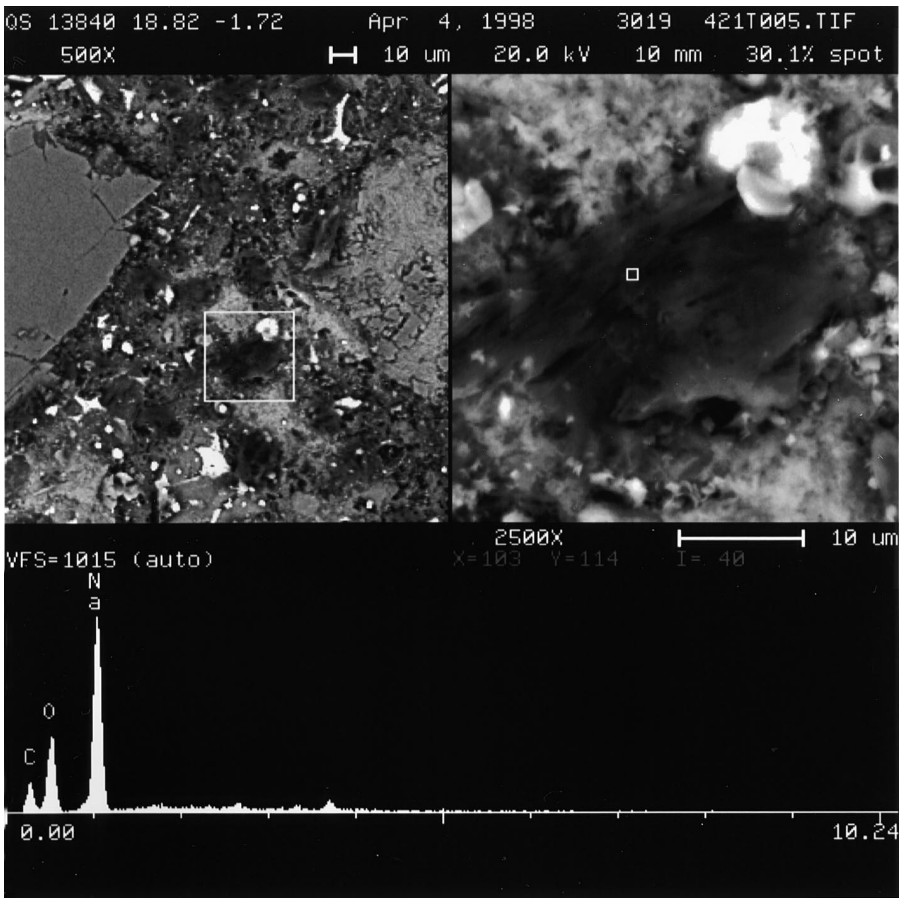

Fig. 5. The microstructure and the EDS spectrum of the Na-rich solid which has crystallized in the concrete. This solid has crystallized in the vicinity of $Ca(OH)_2$.

phase-pure $Mg(OH)_2$. The $Mg(OH)_2$ appears as pseudomorphs of $Ca(OH)_2$ near the paste–aggregate interface. Fig. 2c shows $Mg(OH)_2$ has replaced $Ca(OH)_2$ over an extensive region at the paste–aggregate interfacial zone. Thus, Mg replaces Ca in the former cement grains and in the $Ca(OH)_2$.

It is well known that $Mg(OH)_2$ is highly insoluble at the pH values normally present in pore solutions. Therefore, establishing a mechanism by which Mg is transported throughout the pore structure is of interest.

The basis for this behavior can be understood in the context of the other phases observed in these concretes. Thaumasite was observed to have formed in this concrete and Fig. 3 shows the morphology typical of thaumasite. When observed by SEM on a polished section, thaumasite and ettringite are very similar in appearance. Consequently, it may be difficult to distinguish these by microstructure alone. However, the EDS spectrum for thaumasite in Fig. 3 shows the presence of calcium, silica, and sulfur. Aluminum is absent. While carbonate can be inferred from an elevated carbon peak, signal from the carbon in the epoxy cannot be ruled out. The presence of thaumasite is indicative of the ingress of both sulfate and carbonate. Thaumasite formation approximately 40 mm below the surface indicates the depth to which sufficient carbonate is available in this concrete to form this carbonate-containing solid.

The analysis of a specimen from the stem wall also provides a basis for predicting the mechanism by which Mg has intruded deeply into this concrete. Fig. 4 shows that NaCl has crystallized within the cement paste and at the paste–aggregate interface. Analysis of the other phases present in this specimen indicates the formation of an Na-containing solid for which no other elements heavier than carbon can be observed in the EDS spectrum. The microstructure and the EDS spectrum of this solid are shown in Fig. 5. Although these data alone are insufficient to determine the composition of this Na-containing solid, various observations [1,2,13,14] suggest it may be $Na_3H(CO_3)_2{\cdot}2H_2O$, $NaHCO_3$, or $Na_2CO_3{\cdot}H_2O$. It is noteworthy that Fig. 5 shows the presence of a sodium carbonate within a few microns of $Ca(OH)_2$. If this is an equilibrium assemblage, it suggests that the reaction [Eq. (4)]:

$$Na_{(2-x)}H_xCO_3(nH_2O) + Ca(OH)_2 \Rightarrow CaCO_3 + (2-x)NaOH + H_2O \quad (4)$$

is not favorable.

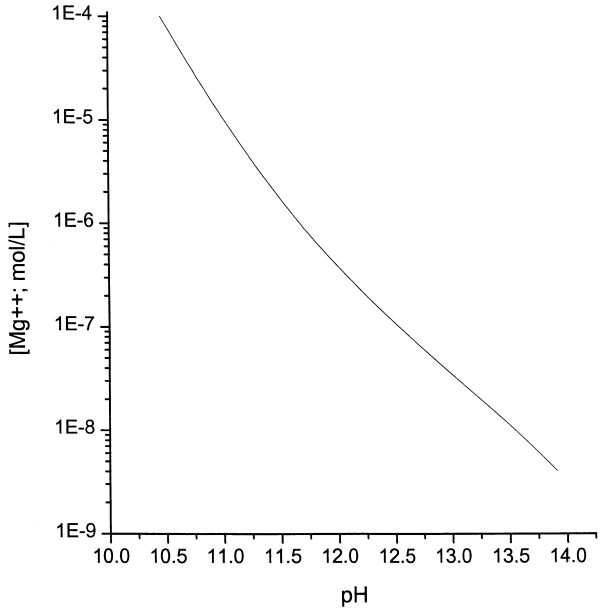

Fig. 6. The variation in the molar solubility of magnesium hydroxide as a function of pH (in the absence of species other than magnesium and hydroxyl).

To establish whether an equilibrium assemblage of phases can involve the co-existence of a sodium carbonate and $Ca(OH)_2$, the speciation code PhreeqC [15] was run. The objective was to determine whether there is an Na ion concentration at which $Ca(OH)_2$ and a sodium carbonate would co-exist in the absence of forming $CaCO_3$. The analysis indicated the co-existence of any solid containing the bicarbonate ion and $Ca(OH)_2$ to be precluded; thus, $NaHCO_3$ (nahcolite) or $NaHCO_3{\cdot}Na_2CO_3{\cdot}2H_2O$ (trona) were determined not to co-exist with $Ca(OH)_2$. The calculation of the conditions needed to precipitate sodium carbonate in the presence of $Ca(OH)_2$, but in the absence of $CaCO_3$, requires an Na concentration greater than 10 M and the pH higher than 16. In that event, the stabilities of $Na_2CO_3{\cdot}H_2O$ (thermonatrite) and $Na_2CO_3{\cdot}10H_2O$ (natron) are approximately comparable. As these conditions are unlikely to exist in concrete, it can be inferred that the sodium carbonate phase observed is present because its precipitation is kinetically favorable and that it will eventually convert to $CaCO_3$ or thaumasite.

Although the observation of NaCl crystals indicates that significant chloride is present in the paste fraction of this concrete, Friedel's salt was not observed within the first 32 mm of the surface. However, Friedel's salt was found distributed throughout the paste at depths below this. The zone where Friedel's salt appeared, correlated with the disappearance of the sodium carbonate phase. Thus, the spatial sequence of solids observed suggests that NaCl from the soil and carbonate from the atmosphere react with solids normally present in concrete to form fronts where sodium carbonate and Friedel's salt are deposited.

As with the formation of thaumasite, the formation of sodium carbonate shows the ingress of carbonate to a significant depth. The presence of these carbonates is also consistent with the reduction in pH. As Fig. 6 shows, the solubility of Mg is strongly dependent on pH. Fig. 6 shows the result of a common ion effect calculation showing the molar concentrations of Mg in solution depending on the hydroxide ion concentration. As the pH is reduced from about 13.5 to about 10.5, the Mg concentration in solution is shown to increase by four orders of magnitude. Thus, the depression of the internal pH of concrete due to carbonation will contribute significantly to the ability of Mg to be transported through its pore structure.

A second factor contributing to Mg transport appears to be the nature of the Mg species. A series of free energy minimization calculations using PhreeqC [15] were carried out to assess the effects of a mixed $MgSO_4$–Na_2SO_4–NaCl solution coming in contact with the pore structure of concrete. The initial solution concentration was taken to be 0.091 M NaCl, 0.044 M Na_2SO_4, and 0.071 $MgSO_4$. These values were obtained from the analyses of soil in the vicinity of the concrete [16]. The effects of pore solutions containing 0.1, 0.01, 0.001 and 0.0001 M NaOH on the solution speciation and on the tendency for $Mg(OH)_2$ to precipitate were calculated. The results obtained are summarized in Table 1.

This table predicts two phenomena observed in the microstructural analysis of these concretes. As the model pore solution becomes more acidic, the saturation index for brucite decreases below saturation and the predominant Mg-containing species in solution becomes the $MgSO_4^\circ$ neutral species. These calculations are consistent with the observed accumulation of sulfate in Mg-rich areas in the microstructure. For example, Fig. 1 showed that Mg replaces Ca in the former belite grains. Such a distribution would be expected in a concrete where the pore solution had become sufficiently acidic to allow the internal transport of Mg. As the Mg approaches a cement grain where the local pH is elevated due to its incomplete hydration, the base exchange reaction shown in Eq. (3) occurs and $Mg(OH)_2$ precipitates.

Table 1
The species in solution and the brucite saturation index depending on the pore solution alkalinity

NaOH	Mg^{2+}	$MgOH^+$	$MgSO_4^\circ$	$NaSO_4^-$	SI[$Mg(OH)_2$]
0.1	9.50×10^{-3}	5.07×10^{-2}	1.08×10^{-2}	2.26×10^{-2}	5.72
0.01	3.04×10^{-2}	7.72×10^{-3}	3.29×10^{-2}	1.40×10^{-2}	3.57
0.001	3.41×10^{-2}	7.92×10^{-4}	3.61×10^{-2}	1.32×10^{-2}	1.54
0.0001	3.45×10^{-2}	7.94×10^{-5}	3.64×10^{-2}	1.29×10^{-2}	−0.47

As an intimate mixture of $Mg(OH)_2$ and $Si(OH)_n$ are incompatible, they may transform to magnesium silicate hydrates as suggested by Gollup and Taylor [8]. Thus, the belite grains undergo the observed conversion to magnesium silicates.

4. Conclusions

The microstructures examined indicate that sodium, magnesium, sulfate, chloride and carbonate have participated in the formation of a variety of phases in concretes subjected to the action of ground water. In particular, magnesium silicate, brucite, Friedel's salt, thaumasite and likely some species of sodium carbonate had formed. The concrete specimens studied were obtained from cores which have not been in direct contact with the soil. Thus, the phases described formed as a result of the transport of sodium, magnesium, sulfate, chloride and carbonate to significant distances through the pore structures of these concretes. These concretes were cast with a water-to-cement ratio in the range of 0.65–0.70. Verbeck and Helmuth [17] predicted that concrete having a water-to-cement ratio in this range is unlikely to develop an effect system of capillary breaks. Present results confirm that prediction.

Acknowledgments

The authors thank James Bothe for running the speciation program.

References

[1] G.A. Novak, A.A. Coleville, Efflorescent mineral assemblages associated with cracked and degraded residential concrete foundations in Southern California, Cem Concr Res 19 (1989) 1.
[2] B.C. Yen, R.E. Bright, Residential Foundation Deterioration Study for the Cities of Lakewood, La Palma, and Cypress, California, California State University, 1990.
[3] H. Haynes, R. O'Neill, P.K. Mehta, Concrete deterioration from physical attack by salts, Concr Int 18 (1) (1996) 671–677.
[4] P.W. Brown, S. Badger, The distributions of bound sulfates and chlorides in concrete subjected to mixed NaCl, $MgSO_4$, Na_2SO_4 attack, in preparation.
[5] N. Thaulow, private communication.
[6] U.H. Jakobsen, V. Johansen, N. Thaulow, Estimating the capillary porosity of cement paste by fluorescent microscopy and image analysis, in: S. Diamond, et. al (Ed.), Microstructure of Cement-Based Systems/Bonding and Interfaces in Cementitious Materials, MRS Symp Proc, Vol. 370, (1995) pp. 226–236.
[7] ASTM Designation C856-95, Standard Practice for Petrographic Examination of Hardened Concrete.
[8] R.S. Gollup, H.F.W. Taylor, Microstructural and microanalytical studies of sulfate attack: I. Ordinary portland cement paste, Cem Concr Res 22 (1992) 1027–1038.
[9] W.F. Cole, A crystalline hydrated magnesium silicate formed in the breakdown of a concrete sea-wall, Nature 171 (1953) 354–355.
[10] D.M. Roy, E. Sonnenthal, R. Prave, Hydrotalcite observed in mortars exposed to sulfate solutions, Cem Concr Res, 15 (1985) 912–916.
[11] D. Bonen, M.D. Cohen, Magnesium sulfate attack on portland cement paste: I. Microstructural analysis, Cem Concr Res 22 (1992) 169–180.
[12] D. Bonen, M.D. Cohen, Magnesium sulfate attack on portland cement paste: II. Chemical and mineralogical analysis, Cem Concr Res 22 (1992) 697–708.
[13] W.F. Cole, C.J. Lancucki, M.J. Sandy, Products form in an aged concrete, Cem Concr Res 11 (1981) 443–454.
[14] D. Bonen, S.L. Sarkar, Environmental attack on concrete, in: G.R. Nisperos, A. Nisperos, J. Bayles (Eds.), Proc. 16th ICMA, ICMA, Duncanville, TX, 1994.
[15] D.L. Parkhurst, PhreeqC: A Computer Program for Speciation, Reaction-Path, Advective-Transport, and Inverse Geochemical Calculations, U.S. Geological Survey, Water Resources Investigations, Report 95-4227, 1995.
[16] J.P. Skalny, private communication.
[17] G.J. Verbeck, R.H. Helmuth, Structures and physical properties of cement paste, Vth ICCC Tokyo, III-1 (1968) 1–32.